

Assigning Temperatures to Eigenstates

Phillip C. Burke,¹ Goran Nakerst,^{2,1} and Masudul Haque^{2,1,3}

¹*Department of Theoretical Physics, Maynooth University, Maynooth, Kildare, Ireland*

²*Institut für Theoretische Physik, Technische Universität Dresden, 01062 Dresden, Germany*

³*Max-Planck Institute for the Physics of Complex Systems, Dresden, Germany*

(Dated: February 3, 2023)

In the study of thermalization in finite isolated quantum systems, an inescapable issue is the definition of temperature. We examine and compare different possible ways of assigning temperatures to energies or equivalently to eigenstates in such systems. A commonly used assignment of temperature in the context of thermalization is based on the canonical energy-temperature relationship, which depends only on energy eigenvalues and not on the structure of eigenstates. For eigenstates, we consider defining temperature by minimizing the distance between (full or reduced) eigenstate density matrices and canonical density matrices. We show that for full eigenstates, the minimizing temperature depends on the distance measure chosen and matches the canonical temperature for the trace distance; however, the two matrices are not close. With reduced density matrices, the minimizing temperature has fluctuations that scale with subsystem and system size but appears to be independent of distance measure. In particular limits, the two matrices become equivalent while the temperature tends to the canonical temperature.

I. INTRODUCTION

In recent years, there has been significant interest in reconciling statistical mechanics to the quantum dynamics of isolated many-body systems. This endeavor invariably requires a correspondence between energy, a quantity well-defined in quantum mechanics, and temperature, which is necessary for a statistical-mechanical description. The eigenstate thermalization hypothesis (ETH) [1–10], a cornerstone of this field, posits that each eigenstate contains information relevant to thermalization. Thus, a natural question is how to assign temperatures to each eigenstate based on information encoded in the eigenstates. In this work, we examine possible ways of doing so.

The standard definition of temperature in statistical mechanics is given by the inverse of the derivative of entropy with respect to energy [11, 12]. For an isolated quantum system, the entropy at energy E is defined as the logarithm of the number of microstates (i.e., eigenstates) with energy E , or energy in a window around E . In finite systems, obtaining this entropy generally requires approximating the density of states.

Within the context of thermalization in finite isolated quantum systems, it is more common to use the canonical temperature-energy relationship to extract temperature from the eigenvalues of the system Hamiltonian. The canonical temperature $T_C = 1/\beta_C$ can be obtained for any energy E by inverting the canonical equation

$$E = \langle H \rangle = \frac{\text{tr}(e^{-\beta_C H} H)}{\text{tr}(e^{-\beta_C H})} = \frac{\sum_j e^{-\beta_C E_j} E_j}{\sum_j e^{-\beta_C E_j}}, \quad (1)$$

where E_j are the eigenvalues of the system Hamiltonian H . This relationship originates in statistical mechanics from the context of a system with a bath, but is widely used in the study of the thermalization of isolated (bathless) quantum systems to obtain an energy-temperature

correspondence [8–10, 13–28]. In the large-size limit, the canonical temperature is, of course, equivalent to that obtained by differentiating the entropy.

Curiously, both of these definitions rely only on the energy eigenvalues, making no reference to the physics of the eigenstates. Therefore, it is of obvious interest to compare the temperatures obtained from eigenstates (β_E and β_S , introduced below) with an eigenvalue-based definition. In this work, we introduce ways of obtaining temperatures from eigenstates and then compare them to the canonical temperature, β_C , widely used in the thermalization literature.

If an eigenstate $|E_n\rangle$ of a many-body system ‘knows’ the temperature corresponding to its energy E_n , then one might naïvely expect that $\rho = |E_n\rangle\langle E_n|$ should be closest to the canonical density matrix (DM) $\rho_C = Z^{-1}e^{-\beta H}$ for that value of the inverse temperature β . (Here $Z = \text{tr} e^{-\beta H}$.) Thus, minimizing the distance $d(\rho, \rho_C)$ between these two DMs as a function of β is one way of assigning a temperature to E_n . We refer to this optimal β as the ‘eigenstate temperature’ β_E . As $|E_n\rangle\langle E_n|$ is the limit of the microcanonical DM for an ultra-narrow energy window, this idea is also related to the equivalence of statistical ensembles [29, 30] — this definition of temperature minimizes the distance between microcanonical and canonical DMs.

It is admittedly over-ambitious to expect the complete eigenstate DM ρ to resemble a Gibbs thermal state ρ_C , since the first is a pure state and the second is a mixed state. The two density matrices cannot be expected to be ‘close’, as we will illustrate in Section III. In real-time dynamics, the common inquiry is whether a local sub-region, rather than the whole system, approaches a thermal state [21, 22, 31–41]. The intuition is that the rest of the system acts as an effective bath, even if the textbook properties of a bath (weak coupling, no memory) are not satisfied. Accordingly, ETH is often formulated in terms of local observables or a spatial frac-

tion of the system [22, 23, 39, 40, 42–47], and similar ideas appear in the approach known as canonical typicality [7, 16, 32, 34, 44, 48–51]. Thus, one expects for thermalizing systems that, if the system is partitioned spatially into A and B , with A smaller, then the reduced DM of subsystem A for an eigenstate, $\rho^A = \text{tr}_B \rho$, should approximate the reduced canonical DM, $\rho_C^A = \text{tr}_B \rho_C$ [23, 44, 46]. Inverting this expectation, we obtain another way of assigning temperatures to eigenstates — use the value of β which minimizes the distance $d(\rho^A, \rho_C^A)$. We call this the ‘subsystem temperature’ β_S .

We find that β_E , which minimizes the distance between canonical DMs ρ_C and eigenstate (or microcanonical) DMs ρ , depends on the distance measure employed. Using distances based on the Schatten p -norm [52–55], we show analytically that the minimizing temperature β_E is equal to p^{-1} times the canonical temperature β_C . Thus, only the trace distance ($p = 1$) gives meaningful physical results; even the well-known Hilbert-Schmidt norm ($p = 2$) would provide a temperature that deviates by a factor of two! Although β_E aligns with β_C for $p = 1$, the two DMs are never close, i.e., even the minimum distance is large.

The subsystem temperature β_S appears numerically to be broadly independent of p and is seen to match the canonical temperature β_C only approximately at finite sizes. Thus for finite systems, the reduced DMs of pure eigenstates can be closer to thermal states at temperatures other than the canonical temperature. The correspondence is shown to improve in the limit where the size of the subsystem complement (B) is large, but not necessarily in other ways of taking the large-size limit.

The paper is laid out as follows. In Section II, we outline the distance measures used to quantify how close two density matrices are and introduce the many-body quantum systems that we will numerically investigate. Following this, we present our results for the eigenstate and subsystem temperatures in Sections III and IV, respectively. In Section V, we outline alternative choices that could have been used in our investigations. Then, in Section VI, we investigate the deviation of the subsystem temperature from the canonical temperature as a system approaches integrability. Finally, in Section VII, we summarize our findings and discuss their relation to existing work. In addition, we outline open questions that remain.

II. PRELIMINARIES

Here we first define an appropriate distance measure between density matrices. This distance measure is to be used in our temperature definitions. Following this, we describe the many-body quantum systems used in numerical calculations. For each system, we provide the relevant quantum Hamiltonian.

A. Distance Measures

To quantify the distance between two DMs, we use the Schatten p -distance, the norm of the difference between the two normalized matrices

$$d_p(\rho, \sigma) = \left\| \frac{\rho}{\|\rho\|_p} - \frac{\sigma}{\|\sigma\|_p} \right\|_p, \quad (2)$$

with the Schatten p -norm given by

$$\|A\|_p = \text{tr}(|A|^p)^{1/p} = \left(\sum_n |s_n|^p \right)^{1/p}, \quad (3)$$

for a Hermitian matrix A and $1 \leq p < \infty$. Here s_n are the singular values of A , and $|A| = \sqrt{A^\dagger A}$. This class of distances includes commonly used measures of distance between DMs, such as the trace distance [56, 57] and the Hilbert-Schmidt (or Frobenius) distance [58–72]. The range of d_p is $[0, 2]$.

The main body of this paper are based on the Schatten p -distances. In Section V A, we will examine briefly how our results are affected if one uses instead the Bures distance [56, 57].

B. Many-body systems

To ensure that the presented results hold generally for chaotic (thermalizing) many-body Hamiltonians with local interactions, we will provide numerical results for three different 1D, and a 2D, non spin conserving, chaotic models. For all systems, we consider a spin- $\frac{1}{2}$ lattice of L sites with open boundary conditions.

The first model is the quantum Ising model, with transverse and longitudinal magnetic fields on every site. The transverse and longitudinal fields have strength h_x and h_z respectively. To remove symmetries of the model, we swap the x and z field strength between the first two sites. The chaotic Ising Hamiltonian is then

$$H_I = \sum_{j=1}^{L-1} S_j^z S_{j+1}^z + \sum_{j=1}^L (h_x(1 - \delta_{j,1})S_j^x + h_z(1 - \delta_{j,2})S_j^z) + h_z S_1^x + h_x S_2^z. \quad (4)$$

The second model is the XXZ-chain with staggered transverse and longitudinal magnetic fields along the even and odd sites respectively. In addition, we break the staggered pattern at the start of the chain by inserting x and z fields on the first and second sites respectively to remove any symmetry. The staggered XXZ-chain Hamiltonian is then

$$H_S = \sum_{j=1}^{L-1} (S_j^x S_{j+1}^x + S_j^y S_{j+1}^y + \Delta S_j^z S_{j+1}^z) + \sum_{\text{even}} h_x S_j^x + \sum_{\text{odd}} h_z S_j^z + h_x S_1^x + h_z S_2^z. \quad (5)$$

The last 1D model we used is the *XXZ*-chain with disordered transverse and longitudinal magnetic fields on every site. In this case, rather than h_z and h_x being uniform across the sites, the on-site strengths h_j, h'_j , are chosen from a uniform distribution $[-W, W]$. The disordered *XXZ*-chain Hamiltonian is then

$$H_D = \sum_{j=1}^{L-1} (S_j^x S_{j+1}^x + S_j^y S_{j+1}^y + \Delta S_j^z S_{j+1}^z) + \sum_{j=1}^L (h_j S_j^z + h'_j S_j^x). \quad (6)$$

For all three 1D models, appropriate parameters were chosen to ensure chaotic level spacing statistics. Namely, $h_z = 0.5$, $h_x = 0.75$ for the Ising model, $h_z = h_x = 0.5$ for the staggered field model, and $W = 0.25$ for the disordered field model.

Finally, the 2D model we use is a square lattice, with *XXZ*-like connections between neighboring spins $\langle j, k \rangle$. In addition, transverse magnetic fields are placed on the sites j_a in one of the sub-lattices available within the bipartite square lattice, in order to break total spin conservation. The square lattice Hamiltonian is given by

$$H_{sq} = \sum_{\langle j, k \rangle} [J_{jk} (S_j^x S_k^x + S_j^y S_k^y) + \Delta_{jk} S_j^z S_k^z] + \sum_{j_a} h_x S_{j_a}^x. \quad (7)$$

To ensure chaotic level spacing statistics, the parameters J_{jk} and Δ_{jk} are drawn randomly from the uniform distribution $[0, 2]$ and $[0, 1]$ respectively. This choice of parameters ensures any symmetries of the lattice are broken.

For 1D systems, the *A* subsystem is taken to be the leftmost L_A sites of the L -site chains. In the 2D square lattice, the *A* subsystem is taken to be the first L_A consecutive sites, starting from a corner of the square and following either a row or column. When this model is used, illustrations of the lattice geometry are provided. For simplicity, we choose systems whose underlying Hilbert space \mathcal{H} has a tensor product structure $\mathcal{H} = \mathcal{H}_A \otimes \mathcal{H}_B$. This is the case for spin and fermionic systems, where total spin and particle number respectively are not conserved. Then the full Hamiltonian can be written as $H = H_A \otimes \mathbb{1}_{D_B} + \mathbb{1}_{D_A} \otimes H_B + H_{AB}$, where H_A and H_B only act on *A* and *B* respectively, and H_{AB} is the interaction between the two. The Hilbert space dimensions of *A*, *B* and the total system are D_A , D_B and $D = D_A D_B$ respectively.

III. EIGENSTATE TEMPERATURE

Here we discuss the eigenstate temperature, which we have defined as

$$\beta_E = \operatorname{argmin}_{\beta} d_p(\rho, \rho_C). \quad (8)$$

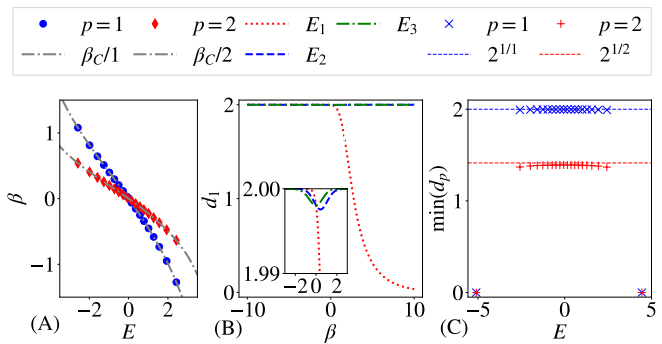


FIG. 1. Eigenstate temperature results for staggered field *XXZ*-chain: $h_x = h_z = 0.5$, $\Delta = 0.95$, $L = 10$. (A) β_E against energy, for 20 eigenstates which are equally spaced in energy across the spectrum, with curves showing β_C/p . (Highest/lowest state not visible.) (B) $d_1(\rho, \rho_C)$ vs β curve for ground state (E_1), mid-spectrum state (E_3), and E_2 in between the two. (C) The minimum of $d_p(\rho, \rho_C)$ plotted against eigenenergy, for the same eigenstates used in (A).

Here, ρ is an eigenstate density matrix, while ρ_C is a canonical density matrix. We first present analytical results that are general to all Hermitian systems. In addition, we provide numerical results that illustrate these analytical results. Following this, we consider a variation of the eigenstate temperature. In particular, we consider a density matrix consisting of an equally weighted sum of eigenstates from a finite energy window, i.e., a microcanonical density matrix. Finally, we provide the full derivation of the analytical results presented.

A. Main Results

In order to determine the value of β_E , we express the two density matrices in the basis for which they are simultaneously diagonalized, and set to zero the derivative of $d_p(\rho, \rho_C)$ with respect to β . The full derivation of the minimum can be found in Section III C, the main result of which is that the minimum is precisely when

$$E_n = \frac{\operatorname{tr}(H e^{-p\beta H})}{\operatorname{tr}(e^{-p\beta H})}. \quad (9)$$

Thus, comparing with the definition (1) of the canonical temperature,

$$\beta_E = \frac{\beta_C}{p}. \quad (10)$$

The eigenstate and canonical temperatures coincide for $p = 1$, while they differ by a factor of p for $p > 1$. This result is purely mathematical and holds for an arbitrary Hermitian matrix H , irrespective of whether H has the interpretation of a many-body Hamiltonian, e.g., even for a random matrix, see results in Appendix A.

Fig. 1 illustrates this relation $\beta_C = p\beta_E$ (A) and the behavior of the distance d_p (B,C), for the staggered field XXZ-chain.

The result $\beta_E = \beta_C$ (for $p = 1$) does not imply that eigenstate DMs $\rho = |E_n\rangle\langle E_n|$ closely resemble canonical states $\rho_C = Z^{-1}e^{-\beta H}$.

We are comparing a pure state to a highly mixed state, i.e., a projection operator (a rank-1 operator) ρ to a full-rank operator ρ_C . So, even the smallest distance between them (at $\beta = \beta_C$) is close to the maximum. The smallest p -distance is in general close to $2^{1/p}$, an analytical result derived in the following Section III C. The minimum is thus very close to the maximum for most eigenstates, as shown in Fig. 1(B,C). The highest/lowest eigenstates are exceptions.

B. Finite Window Eigenstate Temperature

Instead of the eigenstate DM, $\rho = |E_n\rangle\langle E_n|$, one could use the microcanonical DM,

$$\rho_{MC} = \frac{1}{\mathcal{N}} \sum_{E_j \text{ in } \Delta E} |E_j\rangle\langle E_j|, \quad (11)$$

where ΔE is an energy window containing E_n , and \mathcal{N} is the number of states in the window. This might be considered more physical, as we are now comparing two mixed states.

Here, we fix the energy window width, and allow each window to contain a different number of eigenstates. We want to compute the value of β such that the distance $d_p(\rho_{MC}, \rho_C)$ is minimized. We label this minimizing value the finite window eigenstate temperature $\beta_{\Delta E}$. One can follow the same procedure as is detailed in Section III C for the eigenstate temperature, and make the assumption that the energy $E_{MC} = \text{tr}(H\rho_{MC}) = 1/\mathcal{N} \sum_{E_j \in \Delta E} E_j$ of the microcanonical state ρ_{MC} is roughly $E_{MC} \approx E_j \in \Delta E$, which is valid if the energy interval is sufficiently small, and obtain the similar relation that $\beta_C \approx p\beta_{\Delta E}$.

This result is illustrated numerically in Fig. 2, in which we present results for the chaotic Ising model (A-C) and the staggered field XXZ-chain (D-F). In (A,D), we plot $\beta_{\Delta E}$ that minimizes the Schatten p -distance for the given p , along with two canonical β_C curves, versus energy. In (C,F), we plot the value of the minimum distance for the same energy slices as taken in the left figure. Finally, in (B,E) we plot the d_1 distance versus β for three particular energy slices E_1 , E_2 and E_3 . The numerical results again illustrate the derived relation of $\beta_C = p\beta_{\Delta E}$ for the p -distance d_p when taken between a microcanonical and canonical density matrix.

C. Derivation of analytical results

We wish to minimize the Schatten p -distance (2) between the canonical and eigenstate DMs, i.e., $d_p(\rho, \rho_C)$.

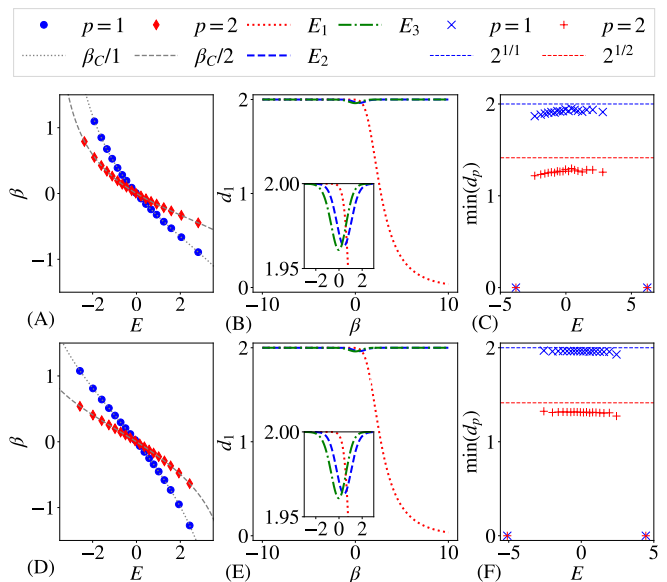


FIG. 2. Finite window eigenstate temperature results for spin chains with $L = 10$, namely: (A)-(C) Chaotic Ising Model with $h_z = 0.5$, $h_x = 0.75$ and $\Delta E \sim 0.059$. (D)-(F) Staggered field XXZ-chain with $\Delta = 0.95$, $J = 1$, $h_x = h_z = 0.5$, and $\Delta E \sim 0.0757$. (A,D) β_{MC} against energy, for 20 energy windows which are equally spaced in energy across the spectrum, with curves showing β_C/p . (Highest/lowest state not visible.) (B,E) $d_1(\rho_{MC}, \rho_C)$ vs β curve for energy windows: E_1 near the ground state, E_2 in the middle of spectrum, and E_3 in between the two. (C,F) The minimum of $d_p(\rho_{MC}, \rho_C)$ plotted against energy, for the same energy windows used in (A,D).

All Schatten p -norms of a matrix ρ can be expressed in terms of the singular values s_n of ρ

$$\|\rho\|_p = \left(\sum_n s_n^p \right)^{1/p}. \quad (12)$$

In other words, the Schatten p -norm is the l_p norm of the singular values. The singular values of a Hermitian matrix ρ are the absolute values of the eigenvalues of ρ . The eigenstate density matrix ρ and the canonical density matrix ρ_C are jointly diagonalizable with respect to the eigenstate basis of H . The eigenvalues of the former are 1 and 0, while the eigenvalues of the latter are given by $e^{-\beta E_j}$, where E_j are the eigenvalues of the Hamiltonian H . The Schatten norms are invariant under a basis transformation by definition, so the normed Schatten p -distance can be written as

$$d_p^p(\rho, e^{-\beta H}) = \left| \frac{1}{\|\rho\|_p} - \frac{e^{-\beta E_n}}{\|e^{-\beta H}\|_p} \right|^p + \sum_{E_j \neq E_n} \frac{e^{-p\beta E_j}}{\|e^{-\beta H}\|_p^p}. \quad (13)$$

Now there are two results we wish to obtain, the value of β for which (13) is minimized, and the value of that minimum. In III C 1 we obtain the surprising result of

$\beta_E = \beta_C/p$, and in III C 2 we determine how the value of the minimum scales.

1. Minimization

To find the minimum of (13), we differentiate the p -normed Schatten p -distance of ρ and $\exp(-\beta H)$ and obtain

$$\begin{aligned} \frac{\partial}{\partial \beta} d_p^p(\rho, e^{-\beta H}) &= -p \left(\frac{1}{\|\rho\|_p} - \frac{e^{-\beta E_n}}{\|e^{-\beta H}\|_p} \right)^{p-1} \\ &\times \frac{\partial}{\partial \beta} \frac{e^{-\beta E_n}}{\|e^{-\beta H}\|_p} + \sum_{E_j \neq E_n} \frac{\partial}{\partial \beta} \frac{e^{-p\beta E_j}}{\|e^{-\beta H}\|_p^p}. \end{aligned} \quad (14)$$

Then, we observe the two derivatives

$$\frac{\partial}{\partial \beta} \frac{e^{-\beta E_n}}{\|e^{-\beta H}\|_p} = \frac{e^{-\beta E_n}}{\|e^{-\beta H}\|_p} \left(-E_n + \frac{\text{tr}(He^{-p\beta H})}{\text{tr}(e^{-p\beta H})} \right) \quad (15)$$

$$\frac{\partial}{\partial \beta} \frac{e^{-p\beta E_j}}{\|e^{-\beta H}\|_p^p} = \frac{pe^{-p\beta E_j}}{\|e^{-\beta H}\|_p^p} \left(-E_j + \frac{\text{tr}(He^{-p\beta H})}{\text{tr}(e^{-p\beta H})} \right). \quad (16)$$

Now, (13) is minimal if and only if (14) is 0, which holds true if and only if

$$\begin{aligned} 0 &= -p \left(\frac{1}{\|\rho\|_p} - \frac{e^{-\beta E_n}}{\|e^{-\beta H}\|_p} \right)^{p-1} \frac{e^{-\beta E_n}}{\|e^{-\beta H}\|_p} \\ &\times \left[-E_n + \frac{\text{tr}(He^{-p\beta H})}{\text{tr}(e^{-p\beta H})} \right] \\ &- p \frac{e^{-p\beta E_n}}{\text{tr}(e^{-p\beta H})} \left[-E_n + \frac{\text{tr}(He^{-p\beta H})}{\text{tr}(e^{-p\beta H})} \right] \\ &- p \frac{\text{tr}(He^{-p\beta H})}{\text{tr}(e^{-p\beta H})} + p \frac{\text{tr}(e^{-p\beta H})}{\text{tr}(e^{-p\beta H})} \frac{\text{tr}(He^{-p\beta H})}{\text{tr}(e^{-p\beta H})}. \end{aligned} \quad (17)$$

The last two terms cancel, and we group the remaining terms together and divide by p to obtain

$$\begin{aligned} 0 &= \left[E_n - \frac{\text{tr}(He^{-p\beta H})}{\text{tr}(e^{-p\beta H})} \right] \\ &\times \left(\left(\frac{1}{\|\rho\|_p} - \frac{e^{-\beta E_n}}{\|e^{-\beta H}\|_p} \right)^{p-1} \frac{e^{-\beta E_n}}{\|e^{-\beta H}\|_p} + \frac{e^{-p\beta E_n}}{\text{tr}(e^{-p\beta H})} \right). \end{aligned} \quad (18)$$

This is zero if and only if

$$E_n = \frac{\text{tr}(He^{-p\beta H})}{\text{tr}(e^{-p\beta H})}. \quad (19)$$

By the one-to-one correspondence of energies and canonical inverse temperatures there exists exactly one β for a given E_n which obeys (19). This β minimizes (13) and we call it β_E . It is related to the canonical inverse temperature β_C , which is defined as the unique solution to (1), via $\beta_C = p \times \beta_E$.

2. Value of the minimum

To allow for the case of using a microcanonical DM in place of the eigenstate DM (III B), we consider the distance (13) with ρ now of the form (11) ($\mathcal{N} = 1$ gives eigenstate temperature). We assume that $\|e^{-\beta H}\|_p \geq \|\rho\|_p e^{-\beta E_j}$, and we separate the final sum into the difference of two sums.

$$\begin{aligned} d_p^p(\rho, e^{-\beta H}) &= \sum_{E_j \in \Delta E} \left(\frac{1}{\mathcal{N}^{1/p}} - \frac{e^{-\beta E_j}}{\|e^{-\beta H}\|_p} \right)^p \\ &+ \sum_{E_j} \frac{e^{-p\beta E_j}}{\|e^{-\beta H}\|_p^p} - \sum_{E_j \in \Delta E} \frac{e^{-p\beta E_j}}{\|e^{-\beta H}\|_p^p}. \end{aligned} \quad (20)$$

Now we consider ρ is constructed from states in the middle of the spectrum, hence we take β close to zero, and we can approximate $e^{-\beta E_j} \approx 1$,

$$\begin{aligned} d_p^p(\rho, e^{-\beta H}) &= \frac{1}{\mathcal{N}} \sum_{E_j \in \Delta E} \left(1 - (\mathcal{N}/D)^{1/p} \right)^p \\ &+ 1 - \sum_{E_j \in \Delta E} \frac{1}{D} \\ &= \left(1 - (\mathcal{N}/D)^{1/p} \right)^p + 1 - \frac{\mathcal{N}}{D}. \end{aligned} \quad (21)$$

If $p = 1$, and we assume $\mathcal{N} \ll D$, it is clear from (21) that $d_1 \approx 2$.

For $p \geq 2$ we use the binomial expansion on (21), and let $D_E = \mathcal{N}/D$,

$$\left(1 - D_E^{1/p} \right)^p = \sum_{n=0}^{\infty} \binom{p}{n} (-1)^n D_E^{n/p} \quad (22)$$

Resulting in

$$d_p^p(\rho, e^{-\beta H}) = 2 - pD_E^{1/p} + O(D_E^\ell) \quad (23)$$

Here, $\ell = \min(1, 2/p)$. Then finally to obtain d_p , we raise both sides to $1/p$, and use the binomial expansion again,

$$d_p(\rho, e^{-\beta H}) = 2^{1/p} - 2^{1/p-1} D_E^{1/p} + O(D_E^\ell) \quad (24)$$

Thus the leading perturbation is $D_E^{1/p} = (\mathcal{N}/D)^{1/p}$. So when $\mathcal{N} \ll D$, d_p is close to $2^{1/p}$ for bulk eigenstates.

IV. SUBSYSTEM TEMPERATURE

We now turn to the subsystem temperature, which we have defined as

$$\beta_S = \underset{\beta}{\text{argmin}} d_p(\rho^A, \rho_C^A). \quad (25)$$

Here, $\rho^A = \text{tr}_B(\rho)$, with ρ an eigenstate DM, and $\rho_C^A = \text{tr}_B(\rho_C)$. The partial trace prevents a calculation similar to that we used to derive $\beta_E = \beta_C/p$; we thus do not have analytical predictions for the relationship between β_S and β_C . On physical grounds, one expects β_S to match β_C for $L_A \ll L$ and large L . We first present our numerical findings for β_S in various quantum systems, exploring this expected correspondence. Following this, we present an analytical argument for how the distance $d_p(\rho^A, \rho_C^A)$, at infinite temperature, should scale in the limit of $L_A \ll L$ and large L .

A. Main Results

The values of β_S are found in general to be scattered around β_C , as shown in Fig. 3(A) for the chaotic Ising model. The width of this scatter generally decreases with system size (both L_A and L), as quantified further below. In stark contrast to β_E , there is no obvious dependence on the distance measure used — the qualitative behavior is the same for all p except $p = \infty$, see Appendix C for $p = 2$ data. We therefore present numerical results for the trace distance, $p = 1$.

The qualitative results of Fig. 3 are not specific to 1D chains. This is clear from the strikingly similar results we obtain for the 2D square lattice model as shown in Fig. 4. In Fig. 4, we illustrate the geometry of the square lattice for each given system/subsystem parameters, alongside the respective β_S and $\min(d_1)$ versus E plots. In the geometry illustrations, the red and black points represent the subsystems A and B respectively. We observe similar results to that of a chaotic 1D spin chain such as those in Fig. 3.

When increasing L_A with fixed total system size L , the variance of β_S and the distance between β_S and β_C decrease, up to $L_A = L/2$. For $L_A > L/2$ the distribution of β_S values changes shape and shows additional features, perhaps resulting from ρ^A no longer having full rank. See Appendix B for examples of results from systems with $L_A > L/2$.

Although $|\beta_S - \beta_C|$ and the variance of β_S improve with increasing L_A , the minimum distance between ρ^A and ρ_C^A does not, as is visible from Figures 3(B) and 4(B). The average $\min(d_1)$ increases markedly with L_A . The reduced DM has decreasing resemblance to the reduced canonical DM, presumably because of the decreasing size of the complement B , which plays the role of a bath.

Increasing L while keeping the fraction L_A/L fixed, we again find the variance of β_S to decrease. In this limit, $\min(d_1)$ on average decreases when the fraction L_A/L is $< \frac{1}{2}$ (see Fig. 3(C)), and is remarkably stable as a function of L when the fraction is $L_A/L = \frac{1}{2}$, see Appendix B.

We now consider fixed L_A and increasing L (or increasing $L_B = L - L_A$). The reduced DMs become increasingly similar in this limit, as shown in Figures 3(D) and 4(C). In Fig. 5 we show scaling behaviors in this limit computed

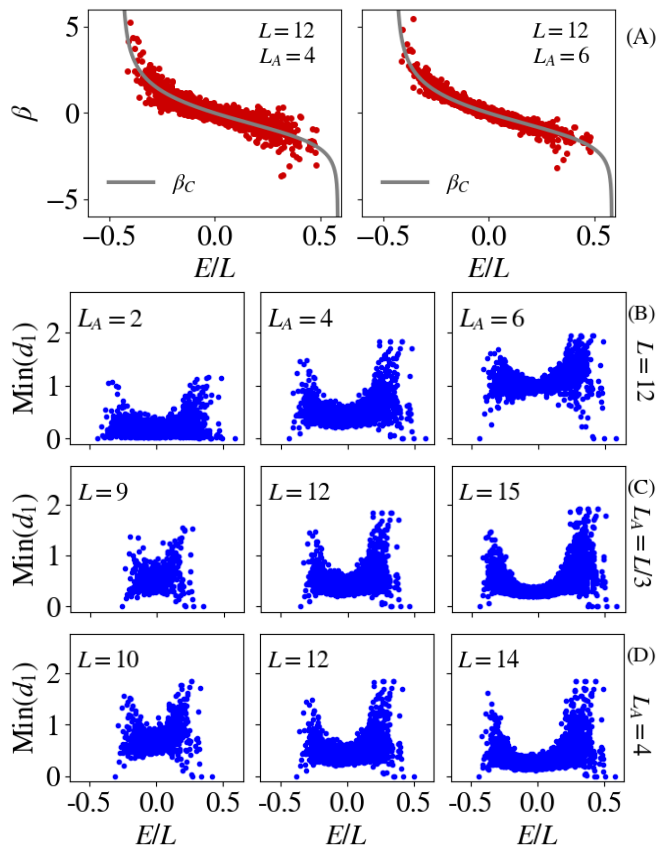


FIG. 3. Subsystem temperature results for the chaotic Ising model with $h_z = 0.5$ and $h_x = 0.75$. (A) β that minimizes $d_1(\rho^A, \rho_C^A)$ (β_S) versus energy, plotted along side the canonical β_C curve, for the given L and L_A . (B)-(D) $\min(d_1(\rho^A, \rho_C^A))$ plotted versus energy, each row illustrating a different scaling of system/subsystem size.

using the central 20% of the spectrum. Fig. 5 (A)-(C) shows results for the disordered-field XXZ-chain, while Fig. 5 (D)-(F) shows those for the chaotic Ising model, both with $L_A = 2$.

The minimum distance between DMs ρ_C^A and ρ^A decreases apparently exponentially with system size, consistent with the upper bound $\sim D_B^{-1/2}$ (equivalently $\sim D^{-1/2}$), see Fig. 5(A)/(D). While this scaling is difficult to prove for a general Hamiltonian, one can argue for this dependence based on assuming the eigenstates to be effectively random Gaussian states near the center of the spectrum. This is known to be a good but not perfect approximation for chaotic many-body systems with local interactions [73–79], and has been used to analyze ETH [2, 10, 17, 42, 43, 45, 74, 80–82]. With this assumption, the reduced DM is a Wishart matrix, while the infinite-temperature canonical DM is an identity matrix. Thus the question is, how fast a p -normalized Wishart matrix concentrates around an identity matrix? Using concentration of measure results [83], one can show that this dependence is at most $D_B^{-1/2}$, as shown in the following

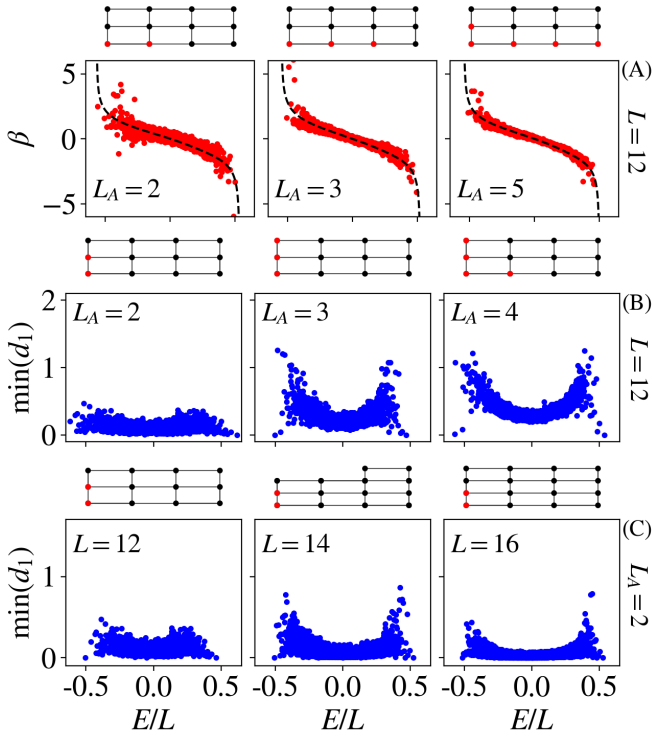


FIG. 4. Subsystem temperature results for square lattice model with the addition of staggered S^x fields with $h_x = 0.5$. The geometry of each system is illustrated above each plot, in which, red and black sites correspond to the subsystems A and B respectively. The results in each plot are of a particular realization - **(A)**: β that minimizes $d_1(\rho^A, \rho_C^A)$ (β_S) versus energy, plotted alongside the canonical β_C curve, for the given L and L_A . **(B-C)**: $\min(d_1(\rho^A, \rho_C^A))$ plotted versus energy, each row illustrating a different scaling of system/subsystem size.

Section IV B.

The width of $\min(d_1)$ clouds appears to decrease at least as fast as $\sim D_B^{-1/2}$ as well, as shown in Fig. 5(A)/(D). This is reasonable as d_1 is bounded from below and the average $\min(d_1)$ decreases as $\sim D_B^{-1/2}$.

The width of the β_S values which minimize d_1 also appears to have $\sim D_B^{-1/2}$ scaling (at most), see Fig. 5(B)/(E). We have been unable to formulate an analytic argument for this scaling. As the width of the β_S cloud decreases, these values concentrate on a line in the $L \rightarrow \infty$ limit. Fig. 5(C)/(F) shows, by plotting the average distance of the β_S cloud to the β_C line, that the asymptotic shape of the β_S cloud coincides with the β_C line. From the available data, it is unclear whether this approach is power-law or exponential in L . Again, no analytical prediction is currently available for this dependence. In Ref. [46], an upper-bound scaling of L^{-1} is derived for a closely related quantity, namely, $d_1(\rho^A, \rho_C^A)$ evaluated at β_C , instead of at its minimum β_S . Fig. 5(C)/(F) shows that the actual scaling of $\min d_1$ is much faster. In Appendix D we calculate the average value of $d_1(\rho^A, \rho_C^A)$ at β_C as a function of L .

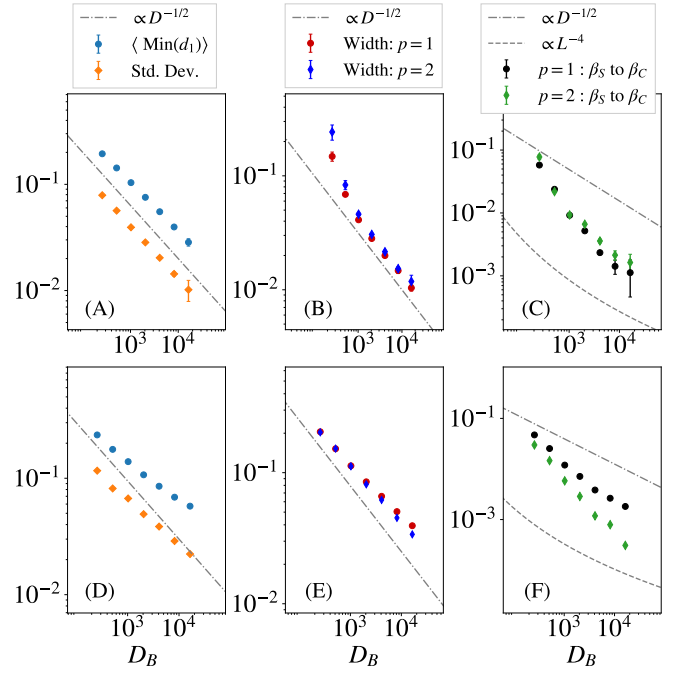


FIG. 5. Subsystem temperature scaling for **(A)-(C)** disordered field XXZ -chain with $W = 0.25$, and $L_A = 2$, over many disorder realizations. **(D)-(F)** chaotic Ising model with $h_x = 0.75$, $h_z = 0.5$, and $L_A = 2$. For both models, statistics are taken from the central 20% of the spectrum. **(A),(D)** Mean of $\min(d_1(\rho^A, \rho_C^A))$ and its standard deviation, vs. D_B for $p = 1$. **(B),(E)** Width of β_S vs. D_B for $p = 1, 2$. **(C),(F)** RMS-distance from the linear fit of β_S , to β_C curve versus D_B , for $p = 1, 2$.

B. Scaling of subsystem distance derivation

In this subsection we will prove that at infinite temperature the Schatten-1 distance between an eigenstate of a generic Hamiltonian and the reduced canonical density matrix decreases as $O(D^{-1/2})$ or equivalently $O(D_B^{-1/2})$ in the limit of fixed subsystem size L_A and increasing complement $L_B \rightarrow \infty$. Recall that $D_B = 2^{L_B}$ and $D = 2^L$, so fixed L_A and increasing L_B (increasing L) is equivalent to fixed D_A and increasing D_B (increasing $D = D_A D_B$).

At infinite temperature the canonical density matrix ρ_C is the maximally entangled state $\rho_C = D^{-1} \cdot \mathbb{1}_D$ and its reduced density matrix is $\rho_C^A = D_A^{-1} \cdot \mathbb{1}_{D_A}$. So the spectrum of $\rho^A - \rho_C^A$ equals the spectrum of ρ^A shifted by the constant D_A^{-1} . The Schatten-1 distance between the reduced eigenstate density matrix and the reduced canonical density matrix can then be written as

$$\left\| \rho^A - \frac{\text{tr}_B e^{\beta H}}{\text{tr}(e^{-\beta H})} \right\|_1 = \sum_{j=1}^{D_A} \left| \lambda_j - \frac{1}{D_A} \right|, \quad (26)$$

where the λ_j denote the eigenvalues of ρ^A .

We assume that an eigenstate $|E\rangle$ of a generic Hamiltonian at infinite temperature is well approximated by a

random state uniformly distributed on the S^{D-1} sphere. For large D the uniform distribution on S^{D-1} is close to a multivariate Gaussian distribution with independent components and mean 0 and variance D^{-1} . Because the density matrix $|E\rangle\langle E|$ has rank 1 the reduced density matrix ρ^A is given by $\rho^A = D^{-1}XX^t$, where X is a $D_A \times D_B$ matrix with independent Gaussian entries with mean 0 and variance 1. The reduced eigenstate density ρ^A is distributed according to the Wishart distribution with expectation value $D_A^{-1} \cdot \mathbb{1}_{D_A} = \rho_C$. So the problem of finding an upper bound for (26) reduces to finding an upper bound on how quickly Wishart matrices concentrate around their mean.

To answer this question we use a concentration of measure result about singular values of Gaussian rectangular matrices X , which can be found in, e.g., [83] (Corollary 7.3.3 and exercise 7.3.4). For $0 < t$ with probability $1 - 2e^{-t^2/2}$ all singular values σ_j of X obey

$$\sqrt{D_B} - \sqrt{D_A} - t \leq \sigma_j \leq \sqrt{D_B} + \sqrt{D_A} + t. \quad (27)$$

The eigenvalues λ_j of $\rho^A = D^{-1}XX^t$ are the squared singular values of X , re-normalized by D^{-1} , namely $\lambda_j = D^{-1}\sigma_j^2$. So for $0 < s < 1 + D_A/D_B - 2\sqrt{D_A/D_B}$ with probability $1 - 2e^{-sD_B/2}$ we have

$$\sum_{j=1}^{D_A} \left| \lambda_j - \frac{1}{D_A} \right| \leq \frac{D_A}{D_B} + 2\frac{\sqrt{D_A}}{\sqrt{D_B}} + s + 2 \left(1 + \frac{\sqrt{D_A}}{\sqrt{D_B}} \right) \sqrt{s}. \quad (28)$$

Note that for fixed D_A the leading order in the s independent term is $D_B^{-1/2}$. Under some mild assumptions on higher moments of λ_j , for example that the second moment of λ_j increases at most polynomially for fixed D_A and increasing D_B , we can asymptotically estimate the expected value of (26) as

$$E \left[\sum_{j=1}^{D_A} \left| \lambda_j - \frac{1}{D_A} \right| \right] \lesssim 2(\sqrt{D_A} + 1)D_B^{-1/2} + O(D_B^{-1}). \quad (29)$$

Thus one expects the Schatten-1 distance between the reduced density matrix of a Gaussian random state and the maximally mixed state to decrease as $O(D_B^{-1/2})$ or equivalently $O(D^{-1/2})$ for fixed D_A and increasing D_B .

V. ALTERNATE FORMULATIONS

Here, we present some possible alternate formulations of our eigenstate-based temperatures. First, we discuss using the Bures distance in place of the Schatten p -distance. We derive an analytical result for the eigenstate temperature utilizing the Bures distance, analogous to that shown in III. Following this, we discuss the use of $\exp(-\beta H_A)$ in place of $\text{tr}(\rho_C)$ in the subsystem temperature. We provide numerical results for this alternate formulation of β_S .

A. Bures Distance

Instead of the Schatten p -distances, one could justifiably use the Bures distance, related to the fidelity [56, 57]. We have found that the subsystem temperature β_S , when calculated using the Bures distance, has the same overall features as found using the Schatten distances.

Additionally, the eigenstate temperature if based on the Bures distance, is the same as β_C , i.e., the same as β_E for $p = 1$. We derive this analytically below, and also illustrate the result numerically.

The fidelity between two density matrices is given as

$$F(\rho, \sigma) = (\text{tr} \sqrt{\rho^{1/2} \sigma \rho^{1/2}})^2, \quad (30)$$

or sometimes as the square root fidelity (quantity fidelity) $F'(\rho, \sigma) = \sqrt{F(\rho, \sigma)}$. It is a measure of how similar ρ and σ are, but it is not a metric on density operators. It is symmetric in the inputs, and is bounded between 0 and 1.

Before delving into maximizing F , we note that the square root of a microcanonical density matrix ρ , as defined in (11), is $\sqrt{\mathcal{N}}\rho$, as

$$(\sqrt{\mathcal{N}}\rho)^2 = \frac{\mathcal{N}}{\mathcal{N}^2} \sum_{E_j, E_{j'} \in \Delta E} |E_j\rangle\langle E_j| E_{j'}\rangle\langle E_{j'}| \quad (31)$$

$$= \frac{1}{\mathcal{N}} \sum_{E_j \in \Delta E} |E_j\rangle\langle E_j| = \rho \quad (32)$$

Now, we want to maximize the fidelity between a microcanonical state $\rho = \rho_{MC}$ and a canonical state ρ_C .

$$F(\rho, \rho_C) = \text{tr} \left(\sqrt{\rho^{1/2} \rho_C \rho^{1/2}} \right)^2 = (\text{tr} \sqrt{\rho \rho_C})^2 \quad (33)$$

$$= \left(\text{tr} \left(\sqrt{\mathcal{N}} \rho e^{-\beta H/2} \right) \right)^2 / \text{tr}(e^{-\beta H}) \quad (34)$$

$$= \frac{1}{\mathcal{N} \text{tr}(e^{-\beta H})} \left(\text{tr} \left(\sum_{E_j \in \Delta E} e^{-\beta E_j/2} |E_j\rangle\langle E_j| \right) \right)^2 \quad (35)$$

$$= \frac{1}{\mathcal{N} \text{tr}(e^{-\beta H})} \left(\sum_{E_j, E_{j'} \in \Delta E} e^{-\frac{\beta}{2}(E_j + E_{j'})} \right) \quad (36)$$

Now to find the value of β which maximizes $F(\rho, \rho_C)$, we simply differentiate to obtain

$$\begin{aligned} \frac{\partial F}{\partial \beta} &= \frac{\text{tr}(H e^{-\beta H})}{\mathcal{N} \text{tr}(e^{-\beta H})^2} \sum_{E_j, E_{j'} \in \Delta E} e^{-\frac{\beta}{2}(E_j + E_{j'})} \\ &+ \frac{1}{\mathcal{N} \text{tr}(e^{-\beta H})} \sum_{E_j, E_{j'} \in \Delta E} -\frac{(E_j + E_{j'})}{2} e^{-\frac{\beta}{2}(E_j + E_{j'})} \end{aligned} \quad (37)$$

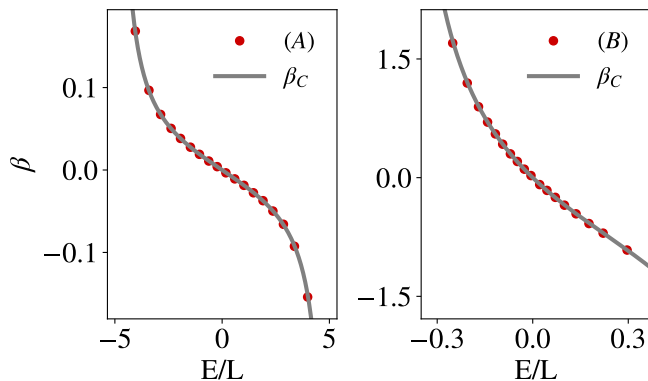


FIG. 6. Finite window eigenstate temperature $\beta_{\Delta E}$ calculated using Bures distance $d_B(\rho_{MC}, \rho_C)$, for two models: **(A)** Random, real and symmetric matrix, **(B)** Chaotic Ising model with $h_x = 0.5$, $h_z = 0.75$. In both cases, $L = 9$ ($D = 2^9$) and 20 energy windows are uniformly chosen from the spectrum of the given Hamiltonian.

$$\frac{\partial F}{\partial \beta} = \frac{1}{\mathcal{N} \text{tr}(e^{-\beta H})^2} \sum_{E_j, E_{j'} \in \Delta E} e^{-\frac{\beta}{2}(E_j + E_{j'})} \times \left(\text{tr}(H e^{-\beta H}) - \frac{E_j + E_{j'}}{2} \text{tr}(e^{-\beta H}) \right) \quad (38)$$

We then make the approximation of $E_j \approx E_{j'} \approx E$ for $E_j, E_{j'} \in \Delta E$, which is accurate for small ΔE , and is exact when ΔE contains a single eigenstate.

$$\frac{\partial F}{\partial \beta} = \frac{e^{-\beta E}}{\text{tr}(e^{-\beta H})} \left(\frac{\text{tr}(H e^{-\beta H})}{\text{tr}(e^{-\beta H})} - E \right) \quad (39)$$

Then setting this equal to zero, we find the only roots of the equation are when

$$E = \frac{\text{tr}(H e^{-\beta H})}{\text{tr}(e^{-\beta H})}. \quad (40)$$

This is the canonical energy-temperature relation (1), meaning that the temperature which maximizes the fidelity between a microcanonical state ρ with energy E , and a canonical state, is in fact the canonical temperature β_C .

The Bures distance is defined as

$$d_B(\rho, \sigma)^2 = 2(1 - \sqrt{F(\rho, \sigma)}), \quad (41)$$

with $F(\rho, \sigma)$ defined as (30). The Bures distance is minimized when the Fidelity is maximized (i.e. when $F = 1$). Thus the Bures distance is minimized when $\beta = \beta_C$ also.

We numerically demonstrate this result in Fig. 6. We present results for both the chaotic Ising model used previously, and also for a random real symmetric matrix, both clearly illustrating the model independent result $\beta_{\Delta E} = \beta_C$ for the Bures distance $d_B(\rho_{MC}, \rho_C)$.

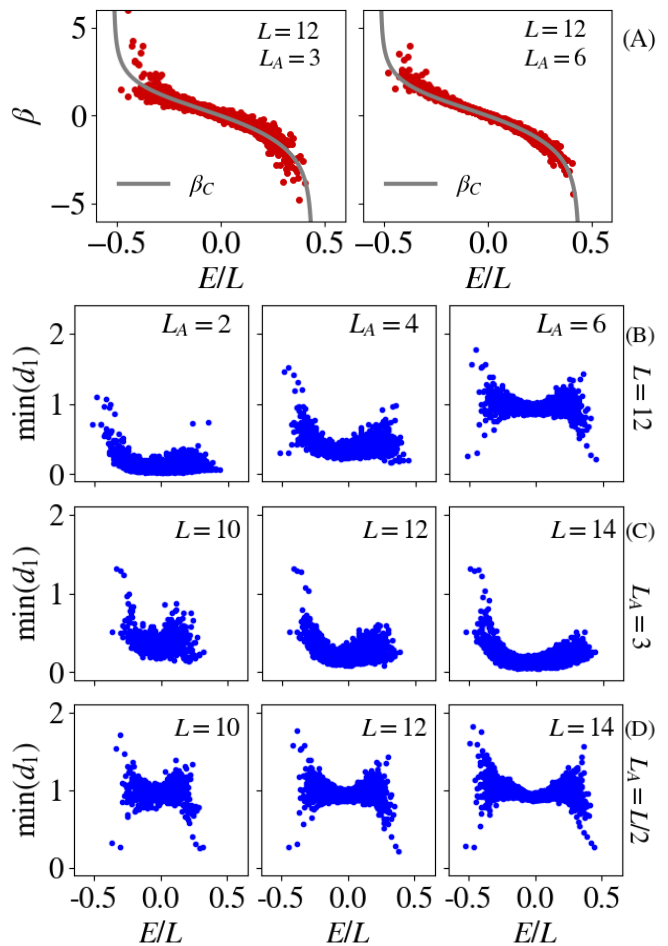


FIG. 7. Subsystem temperature results with $\rho^A = \exp(-\beta H_A)$, for staggered field model with $h_x = h_z = 0.5$, $J = 1$ and $\Delta = 0.95$. **(A)** β minimizing $d_1(\rho^A, \rho_C^A)$ (β_S) versus energy, plotted along side the canonical β_C curve, for the given system/subsystem size. **(B)-(D)** $\min(d_1(\rho^A, \rho_C^A))$ plotted versus energy, each row illustrating a different scaling of system/subsystem size.

B. Local Hamiltonian density matrix

For the subsystem temperature, we compared ρ^A to $\rho_C^A = \text{tr}_B \exp(-\beta H)$. An obvious alternative is to compare with $\exp(-\beta H_A)$. If H_{AB} is nonzero, the two are not equivalent, as discussed widely in the literature [36, 46, 84–94], e.g., in the context of extracting an effective “Hamiltonian of mean force” for the subsystem [84, 85, 91–95]. Numerically, we have found that using $\exp(-\beta H_A)$ to define β_S leads to very similar results to those obtained using ρ_C^A , except for eigenstates at the spectral edges.

In Fig. 7 we illustrate the behavior of β_S and $\min(d_p(\rho^A, \rho_C^A))$ with $\rho_C^A = \exp(-\beta H_A)$. We see the general behavior is the same as in Figures 3 and 4. In Fig. 8 we also illustrate similar scalings as seen in Fig. 5.

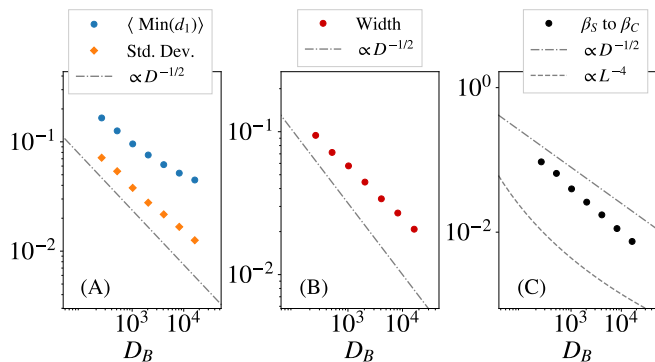


FIG. 8. Subsystem temperature results with $\rho^A = \exp(-\beta H_A)$, for staggered field XXZ -chain with $J = 1$, $\Delta = 0.95$, $h_x = h_z = 0.5$ and $L_A = 2$. Statistics from the central 20% of the spectrum. **(A)** Mean of $\min(d_1(\rho^A, \rho_C^A))$ and its standard deviation, vs. D_B for $p = 1$. **(B)** Width of β_S vs. D_B for $p = 1, 2$. **(C)** RMS-distance from the linear fit of β_S , to β_C curve versus D_B , for $p = 1, 2$.

VI. DEVIATION IN NON-THERMALIZING SYSTEMS

Up to now, we have been solely concerned with chaotic systems that are expected to thermalize and hence satisfy the ETH (ergodic). The subsystem temperature is based on ETH predictions for density matrices restricted to a local subsystem. One could then ask what happens to the temperature in a system that is expected to violate the ETH, i.e., one which does not thermalize (non-ergodic).

In order to investigate this effect, we shall consider the staggered field model with varying field strength $h = h_z = h_x$. For finite, non-zero h , the system should in general be thermalizing. Of course, when $h = 0$ the system is simply the XXZ chain and is known to be exactly solvable via the Bethe ansatz. Thus if we tune h , from some finite non-zero value, towards zero, the system should approach a non-thermalizing regime. In the top panel of Fig. 9 we plot the RMS-distance between β_C and β_S for such a system as a function of magnetic field strength h . As one could expect, when $h \rightarrow 0$ the deviation between the temperatures increases, due to the system no longer thermalizing.

To illustrate the systems approach to a non-thermalizing regime, we have plotted the average restricted gap ratio $\langle \tilde{r} \rangle$ against the field strength h in the bottom panel of Fig. 9. The restricted gap ratio is defined as the minimum of the gap ratio r and its inverse r^{-1} . The gap ratio itself is defined as the ratio of two consecutive level-spacings. Level-spacing statistics are an effective tool in classifying a system as ergodic (chaotic) or non-ergodic (integrable). The restricted gap ratio $\langle \tilde{r} \rangle$ is particularly useful, as it avoids the need to perform an unfolding procedure on the spectrum, as is often required for bare consecutive level-spacings. In the bottom panel of Fig. 9, we have marked the predicted average restricted gap ratio values for chaotic and integrable sys-

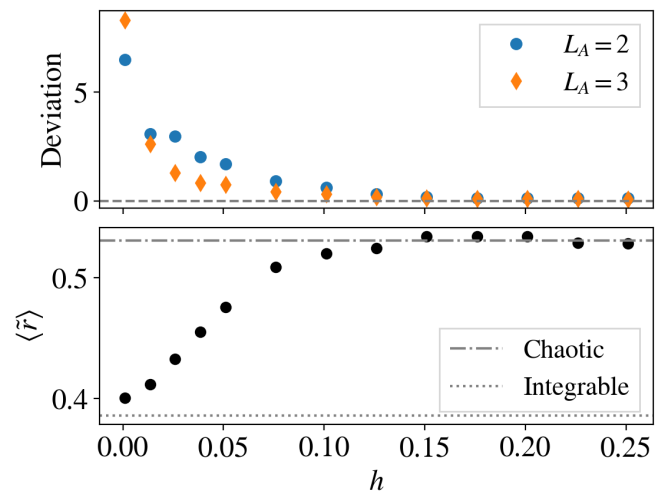


FIG. 9. Subsystem temperature results for staggered field model with $L = 12$, $J = 1$, $\Delta = 0.95$, and $h_z = h_x = h$. **Top:** The RMS-distance between β_S and β_C (Deviation) plotted versus shared field strength h . The RMS-distance is calculated for eigenstates in the central 20% of the spectrum. **Bottom:** Average restricted gap ratio value plotted versus shared field strength h .

tems, 0.5307 and 0.386 respectively [96]. As expected, $\langle \tilde{r} \rangle$ approaches the predicted value for non-ergodic systems as $h \rightarrow 0$, coinciding with the increasing deviation between β_S and β_C .

VII. SUMMARY & DISCUSSION

Our first eigenstate-based temperature, β_E , turned out to be determined solely by the eigenvalues. It has interesting (arguably unexpected) dependencies on the distance measure. The relation $\beta_E = \beta_C/p$ is a mathematical result that holds for any system, including non-chaotic (integrable, many-body-localized,...) systems and even systems without any notion of locality.

In contrast, the second eigenstate-based temperature, β_S , is independent of the distance measure and reflects the physics of the eigenstates. This contrast highlights that the partial trace operation is a crucial ingredient for the emergence of thermodynamics. We have shown that β_S conforms increasingly to β_C when the system size increases while keeping L_A (subsystem size) fixed, and also while keeping the ratio L_A/L fixed to some value smaller than $1/2$. As β_S depends on the chaotic (thermalizing) nature of the system and the physical content of the eigenstates, it does not match β_C for random matrices, as shown in Appendix A, and generally shows deviant behavior for non-chaotic systems (Section VI).

By asking how close ρ^A can be to ρ_C^A , we have characterized the best temperature (typically different from the canonical temperature at finite sizes), and also the degree to which the system is thermal, e.g., through the value of the minimum distance d_1 . The issues ad-

dressed in the investigation of β_S are closely related to (in some sense the converse of) questions addressed in the ETH/thermalization literature, e.g., in Refs. [23, 46, 97–105]. Our results on size dependence confirms the intuition obtained from Refs. [23, 98, 101, 102] that thermal behavior is best seen in the limit of $L_A/L \rightarrow 0$.

The present work raises a number of new questions.

(1) The partial trace and minimization operations in the definition of β_S render analytical treatments difficult. Thus, it remains an open task to prove analytically that β_S should be independent of p , or that it should approach β_C in the large size limit. The latter is consistent with the spirit of ETH, which is similarly difficult to prove, but is verified in a wide array of numerical studies [7, 8, 10, 13–15, 17, 18, 24–28, 42, 43, 45, 74, 78, 80, 81, 106–122]. Proving the $D^{-1/2}$ behavior of Fig. 5(B) also remains an open problem.

(2) The correspondence between β_S and β_C may break down when approaching non-chaotic regimes, such as near-integrability or many-body localization [19, 123, 124]. There is the possibility of scaling with different power-laws than those seen here, in analogy to the power-law ETH scaling displayed by integrable models [42, 43, 115, 125–127]. In Section VI we did observe the deviation of β_S from β_C as the system approached integrability, as one might have expected. A deeper investigation into the effects of integrability and localization is required.

(3) A weak or even zero system-bath coupling is often considered the natural setting for discussing quantum thermalization [36, 49]. In the present context, we did not consider it natural to modify H_{AB} , as we do not *a priori* have a system-bath separation, and the partition into A and B is arbitrary. However, it would be interesting to explore the effect of varying H_{AB} . For the exact limit of $H_{AB} = 0$, the reduced density matrix $\rho_C^A = \text{tr}_B(\rho_C)$ is just $e^{-\beta H_A}$, and the eigenstates of the full system decompose into tensor products of the eigenstates of the two subsystems. Thus the reduced eigenstate density matrix ρ^A is simply $|E_j^A\rangle\langle E_j^A|$, where $|E_j^A\rangle$ are eigenstates of H_A . Thus, if one calculates the subsystem temperature β_S for $H_{AB} = 0$, the resulting temperature is actually the eigenstate temperature of the contributing eigenstate in H_A . Then using the result from Section III this temperature will in fact be β_C/p of the subsystem H_A , as opposed to β_C of the total system. One can still ask how the correspondence between β_S and β_C changes systematically in the $H_{AB} \rightarrow 0$ limit.

(4) In this work, we compared the eigenstate-based temperatures β_E and β_S to the canonical temperature β_C . The canonical temperature is widely used as a standard definition of temperature in the study of thermalization in many-body quantum systems. In the study of statistical mechanics, a standard definition of temperature is the inverse of the derivative of entropy with respect to energy. The possibility of entanglement entropy being representative of the thermal entropy in the large system size limit is often discussed [21, 23, 101, 128, 129].

Ref. [23] investigates the deviation of the entanglement entropy from a canonical entropy in a finite quantum system. One could consider the temperature arising from the entanglement entropy of eigenstates as another possible eigenstate based temperature.

ACKNOWLEDGMENTS

We thank S. Denisov, A. Dymarsky and P. A McClarty for helpful discussions. PCB thanks Maynooth University (National University of Ireland, Maynooth) for funding provided via the John & Pat Hume Scholarship. GN thanks the Irish Research Council for funding provided via the Government of Ireland Postgraduate Scholarship Program (Grant No. GOIPG/2019/58), and acknowledges financial support from the Deutsche Forschungsgemeinschaft (DFG) through SFB 1143 (project-id 247310070). The authors acknowledge the Irish Centre for High-End Computing (ICHEC) for the provision of computational facilities.

APPENDIX

In the appendices, we provide additional numerical results:

- In Appendix A we present numerical results for both the eigenstate and subsystem temperatures, using random matrices in place of a physical Hamiltonian. We illustrate the generality of the analytical result of $\beta_C = p\beta_E$, and also show how poorly β_S and β_C align for random matrices.
- In Appendix B we present further numerical data for the subsystem temperature, in particular, the result of varying the subsystem size in the staggered field model.
- In Appendix C, we present results obtained using the Schatten 2-norm in place of the 1-norm for the subsystem temperature.
- In Appendix D, we compute the distance between ρ^A and ρ_C^A at the canonical temperature β_C .

Appendix A: Random Matrix Results

Here we present the results for both the eigenstate temperature β_E and the subsystem temperature β_S using a random, real, symmetric matrix in place of a physical Hamiltonian.

1. Eigenstate Temperature

As previously demonstrated, $\beta_C = p\beta_E$ is a general mathematical result that will hold for any Hermitian ma-

trix H . Here we illustrate this with a random matrix in Fig. 10.

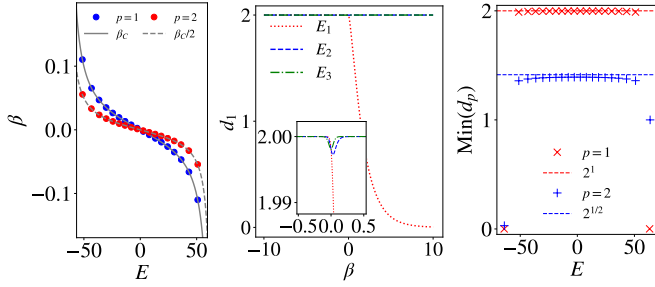


FIG. 10. Eigenstate temperature results for random symmetric matrix with $D = 2^{10}$. **Left:** β_E against energy, for 20 eigenstates which are equally spaced in energy across the spectrum, with curves showing β_C/p . (Highest/lowest state not visible.) **Mid:** $d_1(\rho, \rho_C)$ vs β curve for ground state (E_1), mid-spectrum state (E_3), and E_2 in between the two. **Right:** The minimum of $d_p(\rho, \rho_C)$ plotted against eigenenergy, for the same eigenstates used in (A).

2. Subsystem Temperature

In the main text we found that $|\beta_S - \beta_C| \rightarrow 0$ when $L_A/L \rightarrow 0$, for the chaotic systems that we studied. Here we illustrate in Fig. 11 that this is not a generic result, showing how poorly the temperatures align for a random matrix.

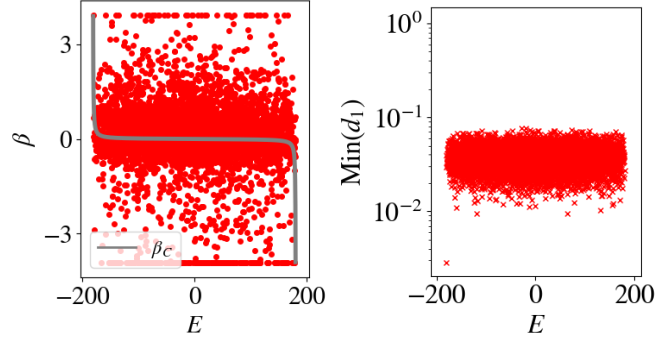


FIG. 11. Subsystem temperature results for a random symmetric matrix with $D = 2^{13}$. **Left:** β minimizing $d_1(\rho^A, \rho_C^A)$ (β_S) versus energy, plotted along side the canonical β_C curve. **Right:** $\min(d_1(\rho^A, \rho_C^A))$ plotted versus energy.

Appendix B: Subsystem Temperature - Various subsystem sizes

Here, we present the result of using different subsystem sizes when computing the subsystem temperature β_S , in various models.

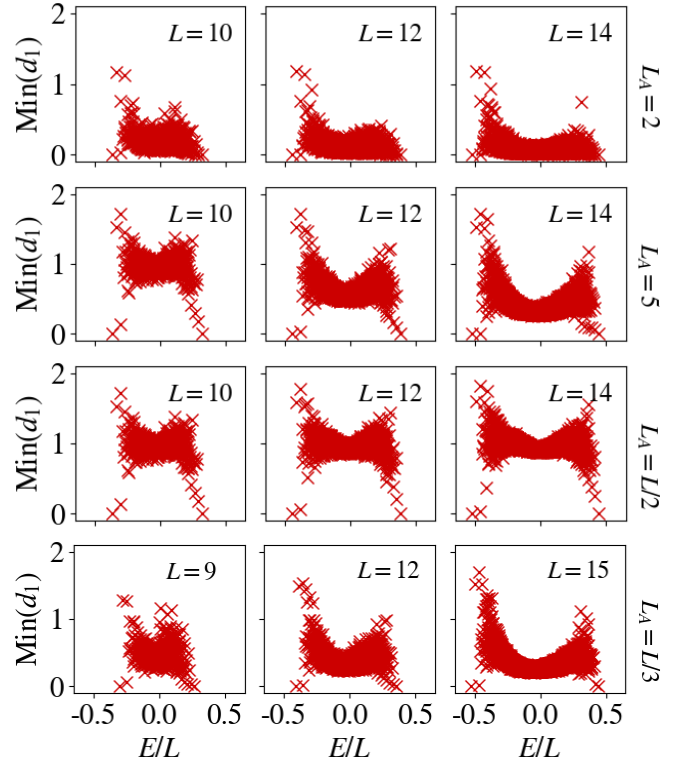


FIG. 12. Subsystem temperature results for staggered field model with $h_x = h_z = 0.5$, $J = 1$ and $\Delta = 0.95$. $\min(d_1(\rho^A, \rho_C^A))$ plotted versus energy for the captioned L and L_A .

In Fig. 12 we show the resultant minimum d_1 when using different subsystem sizes for various system sizes. Illustrating again the decrease in average minimum distance as L increases, but also showing that the average minimum distance increases with increasing L_A .

In Fig. 13 we show the explicit scaling of various quantities. We see in (A) that the average minimum of d_1 increases as L_A increases, i.e., the two matrices become less alike. In (B) the standard deviation of the minima increases but then decreases again as L_A approaches $L/2$. In (C) we see the width of β_S decreased as L_A increased, and similarly in (D) the distance between β_C and β_S decreased as L_A increased.

In the main text, we restricted our results to subsystems with $L_A < L/2$. Here we present an example of the result of using a subsystem with $L_A > L/2$. The minimum distance $\min(d_p(\rho^A, \rho_C^A))$ continues the trend previously described of increasing as L_A increases, and the variance of the values also decreased. However, the β_S values appeared to cease to align with the β_C curve, although the variance did continue to decrease. An example of the resultant β_C for a subsystem greater than half the total system can be seen in Fig. 14. One can also see that the distance between the matrices is close to the maximum value.

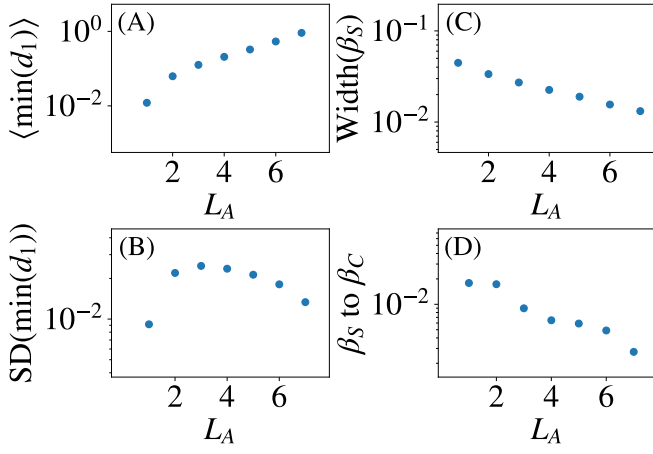


FIG. 13. Subsystem temperature scaling with subsystem size results. Staggered field model with $h_x = h_z = 0.5$, $J = 1$, $\Delta = 0.95$ and $L = 14$. (A) Mean value of $\min(d_1(\rho^A, \rho_C^A))$, (B) Standard deviation of $\min(d_1(\rho^A, \rho_C^A))$, (C) Width of β_S data (D) RMS-distance between β_C and linear fit to β_S , versus L_A . All quantities are calculated in the central 20% of the spectrum.

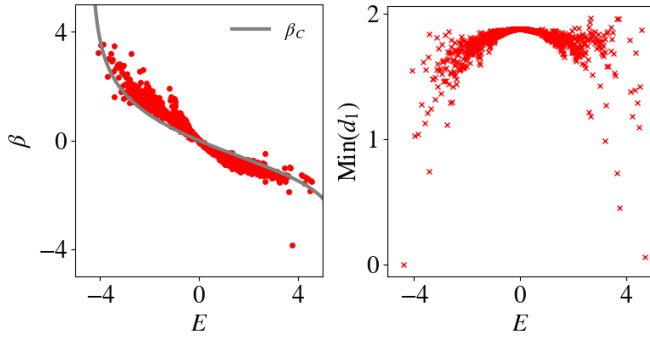


FIG. 14. Subsystem temperature results for chaotic Ising model with $L = 10$ and $L_A = 7$, $h_x = 0.75$ and $h_z = 0.5$. **Left:** β_S vs. E with canonical β_C curve shown. **Right:** $\min(d_1(\rho^A, \rho_C^A))$ versus energy.

Appendix C: Subsystem temperature with alternate p -distances

In the main text, we showed there was an explicit p -distance dependence for the full eigenstate temperature, and stated that we found no similar dependence for the subsystem temperature. In Fig. 15 we show results for the Schatten 2-norm (Hilbert-Schmidt norm). The scaling results that we find are generally the same as those obtained for $p = 1$. The only exception that we found was the $p = \infty$ distance (the operator norm), which resulted in a gap in β_S around $\beta = 0$. Thus, in this case, β_S was never close to β_C where β_C was near zero.

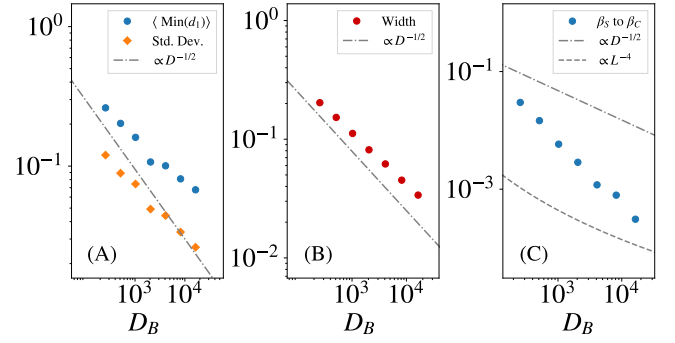


FIG. 15. Subsystem temperature results using $p = 2$ distance, for chaotic Ising model with $h_x = 0.75$, $h_z = 0.5$ and $L_A = 2$. Statistics from the central 20% of the spectrum. (A) Mean of $\min(d_2(\rho^A, \rho_C^A))$ and its standard deviation, vs. D_B . (B) Width of β_S vs. D_B . (C) RMS-distance from the linear fit of β_S , to β_C curve versus D_B .

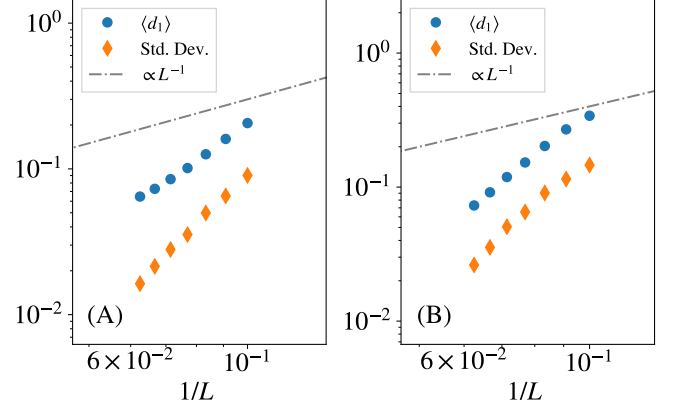


FIG. 16. Distance d_1 at canonical temperature β_C , averaged over the central 20% of the spectrum, versus inverse system size L . We also show the mean standard deviation of the minima. With $L_A = 2$ for (A) Staggered field XXZ-chain, with $h_z = h_x = 0.5$, and (B) Chaotic Ising model with $h_z = 0.5$ and $h_x = 0.75$.

Appendix D: Distance at canonical temperature

In the main text, we minimized the distance between the reduced density matrix $\rho^A = \text{tr}_B |E_n\rangle\langle E_n|$, and the reduced canonical matrix $\rho_C^A = \text{tr}_B \exp(-\beta H)$, as a function of β , to obtain the subsystem temperature β_S . One could instead ask how close the two matrices are at the canonical temperature β_C . In Fig. 16 we show the resulting distances for the two chaotic models investigated in the main text. Alongside the data, we show a line proportional to the inverse system size $1/L$, which clearly illustrates that the distance between the matrices at β_C decreases faster than $1/L$, for these particular systems at least.

-
- [1] J. M. Deutsch, Quantum statistical mechanics in a closed system, *Phys. Rev. A* **43**, 2046 (1991).
- [2] M. Srednicki, Chaos and quantum thermalization, *Phys. Rev. E* **50**, 888 (1994).
- [3] M. Srednicki, Thermal fluctuations in quantized chaotic systems, *Journal of Physics A: Mathematical and General* **29**, L75 (1996).
- [4] M. Srednicki, The approach to thermal equilibrium in quantized chaotic systems, *Journal of Physics A: Mathematical and General* **32**, 1163 (1999).
- [5] P. Reimann, Eigenstate thermalization: Deutsch's approach and beyond, *New Journal of Physics* **17**, 055025 (2015).
- [6] J. Deutsch, Eigenstate thermalization hypothesis, *Reports on Progress in Physics* (2018).
- [7] T. Mori, T. N. Ikeda, E. Kaminishi, and M. Ueda, Thermalization and prethermalization in isolated quantum systems: a theoretical overview, *Journal of Physics B: Atomic, Molecular and Optical Physics* **51**, 112001 (2018).
- [8] M. Rigol, V. Dunjko, and M. Olshanii, Thermalization and its mechanism for generic isolated quantum systems, *Nature* **452**, 854 (2008).
- [9] M. Rigol and M. Srednicki, Alternatives to eigenstate thermalization, *Phys. Rev. Lett.* **108**, 110601 (2012).
- [10] L. D'Alessio, Y. Kafri, A. Polkovnikov, and M. Rigol, From quantum chaos and eigenstate thermalization to statistical mechanics and thermodynamics, *Advances in Physics* **65**, 239 (2016).
- [11] F. Reif, *Fundamentals of statistical and thermal physics* (New York, McGraw-Hill, 1965).
- [12] M. Kardar, *Statistical Physics of Particles* (Cambridge University Press, 2007).
- [13] M. Rigol, Breakdown of thermalization in finite one-dimensional systems, *Phys. Rev. Lett.* **103**, 100403 (2009).
- [14] M. Rigol, Quantum quenches and thermalization in one-dimensional fermionic systems, *Phys. Rev. A* **80**, 053607 (2009).
- [15] M. Rigol and L. F. Santos, Quantum chaos and thermalization in gapped systems, *Phys. Rev. A* **82**, 011604 (2010).
- [16] L. F. Santos, A. Polkovnikov, and M. Rigol, Weak and strong typicality in quantum systems, *Phys. Rev. E* **86**, 010102 (2012).
- [17] C. Neuenhahn and F. Marquardt, Thermalization of interacting fermions and delocalization in Fock space, *Phys. Rev. E* **85**, 060101 (2012).
- [18] S. Sorg, L. Vidmar, L. Pollet, and F. Heidrich-Meisner, Relaxation and thermalization in the one-dimensional Bose-Hubbard model: A case study for the interaction quantum quench from the atomic limit, *Phys. Rev. A* **90**, 033606 (2014).
- [19] R. Nandkishore and D. A. Huse, Many-body localization and thermalization in quantum statistical mechanics, *Annual Review of Condensed Matter Physics* **6**, 15 (2015).
- [20] F. H. L. Essler and M. Fagotti, Quench dynamics and relaxation in isolated integrable quantum spin chains, *Journal of Statistical Mechanics: Theory and Experiment* **2016**, 064002 (2016).
- [21] K. Seki and S. Yunoki, Emergence of a thermal equilibrium in a subsystem of a pure ground state by quantum entanglement, *Phys. Rev. Research* **2**, 043087 (2020).
- [22] A. M. Kaufman, M. E. Tai, A. Lukin, M. Rispoli, R. Schittko, P. M. Preiss, and M. Greiner, Quantum thermalization through entanglement in an isolated many-body system, *Science* **353**, 794 (2016).
- [23] J. R. Garrison and T. Grover, Does a single eigenstate encode the full Hamiltonian?, *Phys. Rev. X* **8**, 021026 (2018).
- [24] L. F. Santos and M. Rigol, Onset of quantum chaos in one-dimensional bosonic and fermionic systems and its relation to thermalization, *Phys. Rev. E* **81**, 036206 (2010).
- [25] G. Roux, Finite-size effects in global quantum quenches: Examples from free bosons in an harmonic trap and the one-dimensional Bose-Hubbard model, *Phys. Rev. A* **81**, 053604 (2010).
- [26] K. R. Fratus and M. Srednicki, Eigenstate thermalization in systems with spontaneously broken symmetry, *Phys. Rev. E* **92**, 040103 (2015).
- [27] J. D. Noh, Eigenstate thermalization hypothesis and eigenstate-to-eigenstate fluctuations, *Phys. Rev. E* **103**, 012129 (2021).
- [28] E. Khatami, G. Pupillo, M. Srednicki, and M. Rigol, Fluctuation-dissipation theorem in an isolated system of quantum dipolar bosons after a quench, *Phys. Rev. Lett.* **111**, 050403 (2013).
- [29] V. Gurarie, The equivalence between the canonical and microcanonical ensembles when applied to large systems, *American Journal of Physics* **75**, 747 (2007).
- [30] H. Tasaki, On the local equivalence between the canonical and the microcanonical ensembles for quantum spin systems, *Journal of Statistical Physics* **172**, 905 (2018).
- [31] M. Cramer, C. M. Dawson, J. Eisert, and T. J. Osborne, Exact relaxation in a class of nonequilibrium quantum lattice systems, *Phys. Rev. Lett.* **100**, 030602 (2008).
- [32] N. Linden, S. Popescu, A. J. Short, and A. Winter, Quantum mechanical evolution towards thermal equilibrium, *Phys. Rev. E* **79**, 061103 (2009).
- [33] A. R. Usha Devi and A. K. Rajagopal, Dynamical evolution of quantum oscillators toward equilibrium, *Phys. Rev. E* **80**, 011136 (2009).
- [34] A. J. Short, Equilibration of quantum systems and subsystems, *New Journal of Physics* **13**, 053009 (2011).
- [35] C. Gogolin, M. P. Müller, and J. Eisert, Absence of thermalization in nonintegrable systems, *Phys. Rev. Lett.* **106**, 040401 (2011).
- [36] A. Riera, C. Gogolin, and J. Eisert, Thermalization in nature and on a quantum computer, *Phys. Rev. Lett.* **108**, 080402 (2012).
- [37] F. G. S. L. Brandão, P. Źwikliński, M. Horodecki, P. Horodecki, J. K. Korbicz, and M. Mozrzykas, Convergence to equilibrium under a random Hamiltonian, *Phys. Rev. E* **86**, 031101 (2012).
- [38] S. Genway, A. F. Ho, and D. K. K. Lee, Thermalization of local observables in small Hubbard lattices, *Phys. Rev. A* **86**, 023609 (2012).
- [39] G. De Palma, A. Serafini, V. Giovannetti, and M. Cramer, Necessity of eigenstate thermalization, *Phys. Rev. Lett.* **115**, 220401 (2015).

- [40] J. Eisert, M. Friesdorf, and C. Gogolin, Quantum many-body systems out of equilibrium, *Nature Physics* **11**, 124 (2015).
- [41] T. Farrelly, F. G. S. L. Brandão, and M. Cramer, Thermalization and return to equilibrium on finite quantum lattice systems, *Phys. Rev. Lett.* **118**, 140601 (2017).
- [42] W. Beugeling, R. Moessner, and M. Haque, Finite-size scaling of eigenstate thermalization, *Phys. Rev. E* **89**, 042112 (2014).
- [43] W. Beugeling, R. Moessner, and M. Haque, Off-diagonal matrix elements of local operators in many-body quantum systems, *Phys. Rev. E* **91**, 012144 (2015).
- [44] M. P. Müller, E. Adlam, L. Masanes, and N. Wiebe, Thermalization and canonical typicality in translation-invariant quantum lattice systems, *Communications in Mathematical Physics* **340**, 499 (2015).
- [45] R. Mondaini and M. Rigol, Eigenstate thermalization in the two-dimensional transverse field Ising model. II. off-diagonal matrix elements of observables, *Phys. Rev. E* **96**, 012157 (2017).
- [46] A. Dymarsky, N. Lashkari, and H. Liu, Subsystem eigenstate thermalization hypothesis, *Phys. Rev. E* **97**, 012140 (2018).
- [47] A. Dymarsky, Mechanism of macroscopic equilibration of isolated quantum systems, *Phys. Rev. B* **99**, 224302 (2019).
- [48] H. Tasaki, From quantum dynamics to the Canonical distribution: General picture and a rigorous example, *Phys. Rev. Lett.* **80**, 1373 (1998).
- [49] S. Goldstein, J. L. Lebowitz, R. Tumulka, and N. Zanghì, Canonical typicality, *Phys. Rev. Lett.* **96**, 050403 (2006).
- [50] S. Popescu, A. J. Short, and A. Winter, Entanglement and the foundations of statistical mechanics, *Nature Physics* **2**, 754 (2006).
- [51] P. Reimann, Typicality for generalized microcanonical ensembles, *Phys. Rev. Lett.* **99**, 160404 (2007).
- [52] A. Laub, *Matrix Analysis for Scientists and Engineers* (Society for Industrial and Applied Mathematics, 2005).
- [53] R. Horn and C. Johnson, *Matrix Analysis* (Cambridge University Press, 2013).
- [54] X. Zhan, *Matrix Theory* (American Mathematical Society, 2013).
- [55] R. Bhatia, *Matrix Analysis* (Springer, 2013).
- [56] S. Barnett, *Quantum Information* (OUP Oxford, 2009).
- [57] M. Nielsen and I. Chuang, *Quantum Computation and Quantum Information* (Cambridge University Press, 2010).
- [58] R. von Baltz, Distance between quantum states and the motion of wave packets, *European Journal of Physics* **11**, 215 (1990).
- [59] L. Knöll and A. Orłowski, Distance between density operators: Applications to the Jaynes-Cummings model, *Phys. Rev. A* **51**, 1622 (1995).
- [60] V. Bužek and M. Hillery, Quantum copying: Beyond the no-cloning theorem, *Phys. Rev. A* **54**, 1844 (1996).
- [61] V. V. Dodonov, O. V. Man'ko, V. I. Man'ko, and A. Wünsche, Energy-sensitive and “classical-like” distances between quantum states, *Phys. Scr.* **59**, 81 (1999).
- [62] V. V. Dodonov, O. V. Man'ko, V. I. Man'ko, and A. Wünsche, Hilbert-Schmidt distance and non-classicality of states in quantum optics, *Journal of Modern Optics* **47**, 633 (2000).
- [63] A. Wünsche, V. Dodonov, O. Man'ko, and V. Man'ko, Nonclassicality of states in quantum optics, *Fortschritte der Physik* **49**, 1117 (2001).
- [64] V. Dodonov and M. Renó, Classicality and anticlassicality measures of pure and mixed quantum states, *Physics Letters A* **308**, 249 (2003).
- [65] P. Marian, T. A. Marian, and H. Scutaru, Distinguishability and nonclassicality of one-mode Gaussian states, *Phys. Rev. A* **69**, 022104 (2004).
- [66] M. G. Genoni and M. G. A. Paris, Quantifying non-Gaussianity for quantum information, *Phys. Rev. A* **82**, 052341 (2010).
- [67] W. Roga, D. Spehner, and F. Illuminati, Geometric measures of quantum correlations: Characterization, quantification, and comparison by distances and operations, *J. Phys. A: Math. Theor.* **49**, 235301 (2016).
- [68] K. Bartkiewicz, V. c. v. Trávníček, and K. Lemr, Measuring distances in Hilbert space by many-particle interference, *Phys. Rev. A* **99**, 032336 (2019).
- [69] P. J. Coles, M. Cerezo, and L. Cincio, Strong bound between trace distance and Hilbert-Schmidt distance for low-rank states, *Phys. Rev. A* **100**, 022103 (2019).
- [70] V. Trávníček, K. Bartkiewicz, A. Černoč, and K. Lemr, Experimental measurement of the Hilbert-Schmidt distance between two-Qubit states as a means for reducing the complexity of machine learning, *Phys. Rev. Lett.* **123**, 260501 (2019).
- [71] S. Kumar, Wishart and random density matrices: Analytical results for the mean-square Hilbert-Schmidt distance, *Phys. Rev. A* **102**, 012405 (2020).
- [72] J. Park, J. Lee, K. Baek, and H. Nha, Quantifying non-Gaussianity of a quantum state by the negative entropy of quadrature distributions, *Phys. Rev. A* **104**, 032415 (2021).
- [73] W. Beugeling, A. Bäcker, R. Moessner, and M. Haque, Statistical properties of eigenstate amplitudes in complex quantum systems, *Phys. Rev. E* **98**, 022204 (2018).
- [74] I. M. Khaymovich, M. Haque, and P. A. McClarty, Eigenstate thermalization, random matrix theory, and Behemoths, *Phys. Rev. Lett.* **122**, 070601 (2019).
- [75] A. Bäcker, M. Haque, and I. M. Khaymovich, Multifractal dimensions for random matrices, chaotic quantum maps, and many-body systems, *Phys. Rev. E* **100**, 032117 (2019).
- [76] G. De Tomasi, I. M. Khaymovich, F. Pollmann, and S. Warzel, Rare thermal bubbles at the many-body localization transition from the Fock space point of view, *Phys. Rev. B* **104**, 024202 (2021).
- [77] M. Srdinšek, T. Prosen, and S. Sotiriadis, Signatures of chaos in nonintegrable models of quantum field theories, *Phys. Rev. Lett.* **126**, 121602 (2021).
- [78] S. Sugimoto, R. Hamazaki, and M. Ueda, Test of the eigenstate thermalization hypothesis based on local random matrix theory, *Phys. Rev. Lett.* **126**, 120602 (2021).
- [79] L. Pausch, E. G. Carnio, A. Rodríguez, and A. Buchleitner, Chaos and ergodicity across the energy spectrum of interacting bosons, *Phys. Rev. Lett.* **126**, 150601 (2021).
- [80] G. P. Brandino, A. De Luca, R. M. Konik, and G. Mussardo, Quench dynamics in randomly generated extended quantum models, *Phys. Rev. B* **85**, 214435 (2012).
- [81] M. Mierzejewski and L. Vidmar, Quantitative impact of integrals of motion on the eigenstate thermalization

- hypothesis, *Phys. Rev. Lett.* **124**, 040603 (2020).
- [82] G. Nakerst and M. Haque, Eigenstate thermalization scaling in approaching the classical limit, *Phys. Rev. E* **103**, 042109 (2021).
- [83] R. Vershynin, *High-Dimensional Probability: An Introduction with Applications in Data Science*, Cambridge Series in Statistical and Probabilistic Mathematics (Cambridge University Press, 2018).
- [84] S. Hilt, B. Thomas, and E. Lutz, Hamiltonian of mean force for damped quantum systems, *Phys. Rev. E* **84**, 031110 (2011).
- [85] C. Jarzynski, Nonequilibrium work theorem for a system strongly coupled to a thermal environment, *Journal of Statistical Mechanics: Theory and Experiment* **2004**, P09005 (2004).
- [86] H. Dong, S. Yang, X. F. Liu, and C. P. Sun, Quantum thermalization with couplings, *Phys. Rev. A* **76**, 044104 (2007).
- [87] M. F. Gelin and M. Thoss, Thermodynamics of a subensemble of a canonical ensemble, *Phys. Rev. E* **79**, 051121 (2009).
- [88] D. Z. Xu, S.-W. Li, X. F. Liu, and C. P. Sun, Non-canonical statistics of a finite quantum system with non-negligible system-bath coupling, *Phys. Rev. E* **90**, 062125 (2014).
- [89] D. Newman, F. Mintert, and A. Nazir, Performance of a quantum heat engine at strong reservoir coupling, *Phys. Rev. E* **95**, 032139 (2017).
- [90] M. Perarnau-Llobet, H. Wilming, A. Riera, R. Gallego, and J. Eisert, Strong coupling corrections in quantum thermodynamics, *Phys. Rev. Lett.* **120**, 120602 (2018).
- [91] M. Campisi, P. Talkner, and P. Hänggi, Fluctuation theorem for arbitrary open quantum systems, *Phys. Rev. Lett.* **102**, 210401 (2009).
- [92] U. Seifert, First and second law of thermodynamics at strong coupling, *Phys. Rev. Lett.* **116**, 020601 (2016).
- [93] P. Strasberg, G. Schaller, N. Lambert, and T. Brandes, Nonequilibrium thermodynamics in the strong coupling and non-markovian regime based on a reaction coordinate mapping, *New Journal of Physics* **18**, 073007 (2016).
- [94] T. G. Philbin and J. Anders, Thermal energies of classical and quantum damped oscillators coupled to reservoirs, *Journal of Physics A: Mathematical and Theoretical* **49**, 215303 (2016).
- [95] J. G. Kirkwood, Statistical mechanics of fluid mixtures, *The Journal of Chemical Physics* **3**, 300 (1935), <https://doi.org/10.1063/1.1749657>.
- [96] Y. Y. Atas, E. Bogomolny, O. Giraud, and G. Roux, Distribution of the ratio of consecutive level spacings in random matrix ensembles, *Phys. Rev. Lett.* **110**, 084101 (2013).
- [97] M. P. Müller, D. Gross, and J. Eisert, Concentration of measure for quantum states with a fixed expectation value, *Communications in Mathematical Physics* **303**, 785 (2011).
- [98] H.-H. Lai and K. Yang, Entanglement entropy scaling laws and eigenstate typicality in free fermion systems, *Phys. Rev. B* **91**, 081110 (2015).
- [99] C. Tian, K. Yang, P. Fang, H.-J. Zhou, and J. Wang, Hidden thermal structure in Fock space, *Phys. Rev. E* **98**, 060103 (2018).
- [100] Z. Lenarčič, E. Altman, and A. Rosch, Activating many-body localization in solids by driving with light, *Phys. Rev. Lett.* **121**, 267603 (2018).
- [101] T.-C. Lu and T. Grover, Renyi entropy of chaotic eigenstates, *Phys. Rev. E* **99**, 032111 (2019).
- [102] C. Murthy and M. Srednicki, Structure of chaotic eigenstates and their entanglement entropy, *Phys. Rev. E* **100**, 022131 (2019).
- [103] Z. Lenarčič, O. Alberton, A. Rosch, and E. Altman, Critical behavior near the many-body localization transition in driven open systems, *Phys. Rev. Lett.* **125**, 116601 (2020).
- [104] M. Kourehpaz, S. Donsa, F. Lackner, J. Burgdörfer, and I. Březinová, Tuning canonical typicality by quantum chaos, *arXiv* (2021), [arXiv:2103.05974 \[quant-ph\]](https://arxiv.org/abs/2103.05974).
- [105] C. Fleckenstein and M. Bukov, Thermalization and prethermalization in periodically kicked quantum spin chains, *Phys. Rev. B* **103**, 144307 (2021).
- [106] G. Biroli, C. Kollath, and A. M. Läuchli, Effect of rare fluctuations on the thermalization of isolated quantum systems, *Phys. Rev. Lett.* **105**, 250401 (2010).
- [107] R. Steinigeweg, J. Herbrych, and P. Prelovšek, Eigenstate thermalization within isolated spin-chain systems, *Phys. Rev. E* **87**, 012118 (2013).
- [108] R. Steinigeweg, A. Khodja, H. Niemeyer, C. Gogolin, and J. Gemmer, Pushing the limits of the eigenstate thermalization hypothesis towards mesoscopic quantum systems, *Phys. Rev. Lett.* **112**, 130403 (2014).
- [109] H. Kim, T. N. Ikeda, and D. A. Huse, Testing whether all eigenstates obey the eigenstate thermalization hypothesis, *Phys. Rev. E* **90**, 052105 (2014).
- [110] D. J. Luitz and Y. Bar Lev, Anomalous thermalization in ergodic systems, *Phys. Rev. Lett.* **117**, 170404 (2016).
- [111] R. Mondaini, K. R. Fratus, M. Srednicki, and M. Rigol, Eigenstate thermalization in the two-dimensional transverse field Ising model, *Phys. Rev. E* **93**, 032104 (2016).
- [112] T. Yoshizawa, E. Iyoda, and T. Sagawa, Numerical large deviation analysis of the eigenstate thermalization hypothesis, *Phys. Rev. Lett.* **120**, 200604 (2018).
- [113] T. LeBlond, K. Mallayya, L. Vidmar, and M. Rigol, Entanglement and matrix elements of observables in interacting integrable systems, *Phys. Rev. E* **100**, 062134 (2019).
- [114] D. Jansen, J. Stolpp, L. Vidmar, and F. Heidrich-Meisner, Eigenstate thermalization and quantum chaos in the Holstein polaron model, *Phys. Rev. B* **99**, 155130 (2019).
- [115] M. Haque and P. A. McClarty, Eigenstate thermalization scaling in Majorana clusters: From chaotic to integrable Sachdev-Ye-Kitaev models, *Phys. Rev. B* **100**, 115122 (2019).
- [116] M. Brenes, J. Goold, and M. Rigol, Low-frequency behavior of off-diagonal matrix elements in the integrable XXZ chain and in a locally perturbed quantum-chaotic XXZ chain, *Phys. Rev. B* **102**, 075127 (2020).
- [117] M. Brenes, T. LeBlond, J. Goold, and M. Rigol, Eigenstate thermalization in a locally perturbed integrable system, *Phys. Rev. Lett.* **125**, 070605 (2020).
- [118] T. LeBlond and M. Rigol, Eigenstate thermalization for observables that break Hamiltonian symmetries and its counterpart in interacting integrable systems, *Phys. Rev. E* **102**, 062113 (2020).
- [119] J. Richter, A. Dymarsky, R. Steinigeweg, and J. Gemmer, Eigenstate thermalization hypothesis beyond standard indicators: Emergence of random-matrix behavior at small frequencies, *Phys. Rev. E* **102**, 042127 (2020).

- [120] F. Fritzsche and T. Prosen, Eigenstate thermalization in dual-unitary quantum circuits: Asymptotics of spectral functions, *Phys. Rev. E* **103**, 062133 (2021).
- [121] Q. Li, J.-L. Ma, and L. Tan, Eigenstate thermalization and quantum chaos in the Jaynes-Cummings Hubbard model, *Physica Scripta* **96**, 125709 (2021).
- [122] C. Schönle, D. Jansen, F. Heidrich-Meisner, and L. Vidmar, Eigenstate thermalization hypothesis through the lens of autocorrelation functions, *Phys. Rev. B* **103**, 235137 (2021).
- [123] V. Oganesyan and D. A. Huse, Localization of interacting fermions at high temperature, *Phys. Rev. B* **75**, 155111 (2007).
- [124] F. Alet and N. Laflorencie, Many-body localization: An introduction and selected topics, *Comptes Rendus Physique* **19**, 498 (2018).
- [125] S. Ziraldo and G. E. Santoro, Relaxation and thermalization after a quantum quench: Why localization is important, *Phys. Rev. B* **87**, 064201 (2013).
- [126] V. Alba, Eigenstate thermalization hypothesis and integrability in quantum spin chains, *Phys. Rev. B* **91**, 155123 (2015).
- [127] S. Nandy, A. Sen, A. Das, and A. Dhar, Eigenstate Gibbs ensemble in integrable quantum systems, *Phys. Rev. B* **94**, 245131 (2016).
- [128] J. M. Deutsch, Thermodynamic entropy of a many-body energy eigenstate, *New Journal of Physics* **12**, 075021 (2010).
- [129] J. M. Deutsch, H. Li, and A. Sharma, Microscopic origin of thermodynamic entropy in isolated systems, *Phys. Rev. E* **87**, 042135 (2013).